From Photonic Crystal to Subwavelength Micropillar Array Terahertz Lasers

Michael Krall, Martin Brandstetter, Christoph Deutsch, Hermann Detz, Aaron Maxwell Andrews, Werner Schrenk, Gottfried Strasser, and Karl Unterrainer

(Invited Paper)

***Abstract*—We investigate terahertz quantum cascade lasers with a dense array of active micropillars forming the gain medium. Depending on the size of these pillars relative to the emission wavelength different optical regimes are identified. For pillar dimensions on the order of the emission wavelength, a photonic crystal resonator is created. Single mode emission is observed at high symmetry points of the photonic band structure. The selection mechanism of the favored laser mode is studied by analyzing the gain enhancement effect for eigenmodes with a low group velocity and a large mode confinement of the electric field energy in the micropillars. Subwavelength micropillar arrays constitute a photonic metamaterial, which can be described using an effective medium approximation. Similar to a bulk laser ridge, the array forms a Fabry–Pérot resonator that is defined by the boundaries of the array. From the longitudinal mode spacing, we derive an effective group index of the pillar medium. Limitations in terms of minimum filling factors and waveguide losses for the realization of subwavelength micropillar and nanowire array terahertz quantum cascade lasers are investigated.**

***Index Terms*—Photonic crystals, optical metamaterials, optical waveguides, terahertz, quantum cascade lasers.**

I. Introduction

PHOTONIC crystal (PhC) structures can be used to precisely engineer the optical feedback mechanism in semiconductor lasers. Such PhC lasers have been realized for a wide range of emission wavelengths spanning all the way from the blue-violet to the far-infrared [1]–[5]. The typical length scale for the elements of these periodic structures is on the order of the emission wavelength. Common approaches to achieve the required refractive index contrast are to fabricate a regular array of active pillars or to etch holes in the gain medium.

A periodic two-dimensional (2-D) PhC can create a pronounced photonic band gap with no propagating modes similar to a 1-D distributed Bragg reflector. Frequency selective, low loss optical resonators can be formed by realizing external mirrors [6], [7], or by introducing defects in an otherwise regular array of holes [8], [9]. PhCs can also be used to design a 2-D distributed feedback laser. The optical gain is significantly enhanced at the photonic band edges due to the low group velocity and the high confinement of mode energy in the active pillar medium [10], resulting in low threshold currents and single-mode emission of terahertz PhC lasers [3].

A 2-D PhC is in principle periodic in two directions (x-y) and has an infinite extend in the third direction (z). The required vertical mode confinement in z-direction can be realized either using dielectric or plasmonic waveguide concepts. Semiconductor terahertz lasers typically use double-metal or surface plasmon waveguides [11]. In this case, the periodic refractive index variation of a PhC can also be achieved by structuring the top metal waveguide layer [5], [12]. This approach allows not only the control of the optical feedback, but also a vertical optical outcoupling from the cavity. A similar concept has been used for pillar-based devices [13].

Terahertz PhC lasers have been realized using micropillar arrays with a significant refractive index contrast between pillar and host medium in order to introduce a pronounced photonic band gap. Single mode lasing has been observed at the band edges and saddle points in the first and second band of transverse-magnetic (TM) modes [3], [4], [14]. Recently, lasing emission in the effective medium regime has been realized with high density subwavelength micropillar arrays, which exhibited only local band gaps [15]. In this case, the subwavelength structures effectively form an active photonic metamaterial with a permittivity equal to the weighted average of the pillar and host medium.

Quantum cascade active regions, which can be designed for lasing frequencies from the mid-infrared [16] to the terahertz [17], have been used for the pillar medium in these devices. At low temperatures such quantum cascade laser (QCL) structures provide optical gain in the terahertz spectral range. However, due to the low photon energies in the terahertz, the characteristic thermal energy $k_B \cdot T$ exceeds the transition energies already at temperatures significantly below room temperature [18]. Non-radiative scattering of electrons from the upper laser level and back-filling of the lower laser level significantly

Manuscript received February 6, 2015; revised March 26, 2015; accepted March 27, 2015. Date of publication April 2, 2015; date of current version May 19, 2015. This work was supported by the Austrian Scientific Fund FWF (SFB-IRON F25, DK CoQuS W1210), the Austrian NANO Initiative (PLATON), and the Society for Micro- and Nanoelectronics GMe.

M. Krall, M. Brandstetter, C. Deutsch, and K. Unterrainer are with the Photonics Institute and the Center for Micro- and Nanostructures, Vienna University of Technology, 1040 Vienna, Austria (e-mail: michael.krall@tuwien.ac.at; martin.brandstetter@tuwien.ac.at; christoph.deutsch@tuwien.ac.at; karl.unterrainer@tuwien.ac.at).

H. Detz is with the Austrian Academy of Sciences, 1010 Vienna, Austria and also with the Center for Micro- and Nanostructures, Vienna University of Technology, 1040 Vienna, Austria (e-mail: hermann.detz@tuwien.ac.at).

A. M. Andrews and G. Strasser are with the Institute of Solid State Electronics and the Center for Micro- and Nanostructures, Vienna University of Technology, 1040 Vienna, Austria (e-mail: aaron.andrews@tuwien.ac.at; gottfried.strasser@tuwien.ac.at).

W. Schrenk is with the Center for Micro- and Nanostructures, Vienna University of Technology, 1040 Vienna, Austria (e-mail: werner.schrenk@tuwien.ac.at).

Color versions of one or more of the figures in this paper are available online at http://ieeexplore.ieee.org.

Digital Object Identifier 10.1109/JSTQE.2015.2419216

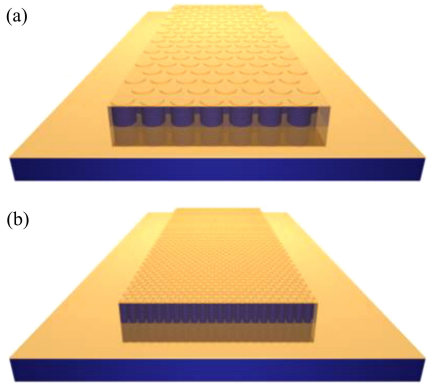

Fig. 1. Scaling of micropillar-based terahertz lasers from PhC lasers to subwavelength pillar arrays. The periodic two-dimensional arrays of micropillars are embedded in a double-metal waveguide for the vertical mode confinement. (a) PhC terahertz laser with pillar dimensions on the order of the emission wavelength. (b) Subwavelength micropillar array terahertz laser.

increases with temperature, limiting the maximum operating temperature [19]. A possible approach to increase the maximum operating temperature of terahertz QCLs is to introduce an additional quantum mechanical confinement in the plane of the semiconductor superlattice, which increases the upper-state life time [20], [21]. This can be achieved by fabricating nanowires with diameters below 100 nm [22]. Therefore, a significant increase of the optical gain is expected if the micropillars of a PhC laser are scaled down to nanowire dimensions. Recently, spontaneous emission in the terahertz from nanowire arrays has been observed [23]. In the optical regime GaN-based nanowire array lasers with electrical injection and dielectric mode confinement have been realized [24].

In this work, we have studied different aspects and limitations regarding the scaling of micropillar array terahertz lasers from PhC to subwavelength pillar dimensions (see Fig. 1). Although the micropillar fabrication can also influence the electronic transport in the device [15], we focus on the optical effects on the laser cavity. These results also reveal important limitations for the realization of nanowire-based terahertz lasers.

II. Gain Enhancement in Active Micropillar Arrays

An important aspect in the scaling of micropillar array terahertz lasers is the mechanism of gain enhancement, which is responsible for the mode selection in PhC lasers. We have evaluated the validity of a 2-D model for a lossless micropillar array, and have studied the influence of material losses on the device operation. Due to the required coupling to intersubband transitions in the quantum cascade structure, only TM eigenmodes have been taken into account in this analysis. In accordance with the experimentally studied devices, the active pillar material has been considered to be surrounded by a benzocyclobutene (BCB) host material, which is commonly used for terahertz applications because of its relatively low absorption losses, and embedded between gold metal waveguide layers for the vertical mode confinement (see Fig. 1).

A. Gain Enhancement in Lossless PhCs

We have calculated the eigenmodes of an infinite periodic array of micropillars in a double-metal waveguide (full 3-D geometry) using a finite element model for the unit cell of the pillar lattice as illustrated in Fig. 2(a) and Bloch periodic boundary conditions. For comparison, we have performed this calculation also for a periodic array of infinitely long pillars (2-D geometry) with the same parameters. Losses in the metal waveguide layers and the host material have been neglected in these calculations.

The TM eigenmodes shown in Fig. 2(b) have been determined for a hexagonal array of GaAs pillars ($\varepsilon_{\mathrm{pillar}} = 13.32$ [25]) in a dielectric BCB host material ($\varepsilon_{\mathrm{host}} = 2.43$ [26]), where the ratio between pillar radius (r) and lattice spacing (a) has been set to $r/a = 0.45$. In the 2-D geometry the normalized eigenfrequencies (fa/c) are strictly independent of the absolute dimensions, and therefore remain unaffected by scaling the micropillar array towards smaller pillar diameters. In the 3-D geometry the normalized eigenfrequencies in principle also depend on the height of the pillars (h). In the calculation a waveguide thickness equal to the pillar diameter has been assumed, which corresponds to $r/h = 0.5$.

The resulting eigenfrequencies for the lowest TM bands are strongly subwavelength with respect to the height of the double-metal waveguide, and therefore the electric field is nearly constant along the z-direction. The electric field distributions in the xy-plane of different modes at high symmetry points of the hexagonal lattice are shown in Fig. 2(c). Results of the 2-D model agree very well with the 3-D calculation, which confirms the validity of the 2-D approximation in the limit of strongly confined eigenmodes of lossless PhC s. In this limit the eigenfrequencies can be considered to be independent of the waveguide thickness. Hence, the normalized photonic bandstructure remains constant for scaling the pillar diameter while keeping the height of the waveguide fixed.

The effect of gain enhancement in active micropillar arrays can be quantified by the ratio of the modal gain to the gain in the pillar medium. Optical gain in the pillars is modeled with a small imaginary component of the permittivity, and in order to correctly account for the coupling to intersubband transitions an anisotropic complex permittivity tensor has been used for the pillar medium. The modal gain has then been determined from the complex eigenfrequency of the mode.

The gain enhancement is influenced by two factors: the velocity of energy-transport through the pillar array, and the electric field energy confinement in the pillar medium. The energy-transport velocity (v_E) of each mode is given by the ratio between the electro-magnetic energy flux (S) and electro-magnetic energy density (W), both averaged in time and over the unit cell:

$$v_E = \frac{\int \mathbf{S}\left(\mathbf{r}\right) dV}{\int \mathbf{W}\left(\mathbf{r}\right) dV}. \tag{1}$$

In the case of lossless, non-dispersive media it is equivalent to the group velocity. The electric field energy confinement (Γ_{Energy}) in the pillar is quantified by the fraction of electric field energy inside the pillar relative to the total electric field

$$\Gamma_{Energy} = \frac{\int_{\varepsilon=\varepsilon_{\mathrm{pillar}}} \varepsilon(\mathbf{r}) \left|\mathbf{E}\left(\mathbf{r}\right)\right|^2 dV}{\int \varepsilon(\mathbf{r}) \left|\mathbf{E}\left(\mathbf{r}\right)\right|^2 dV}. \tag{2}$$

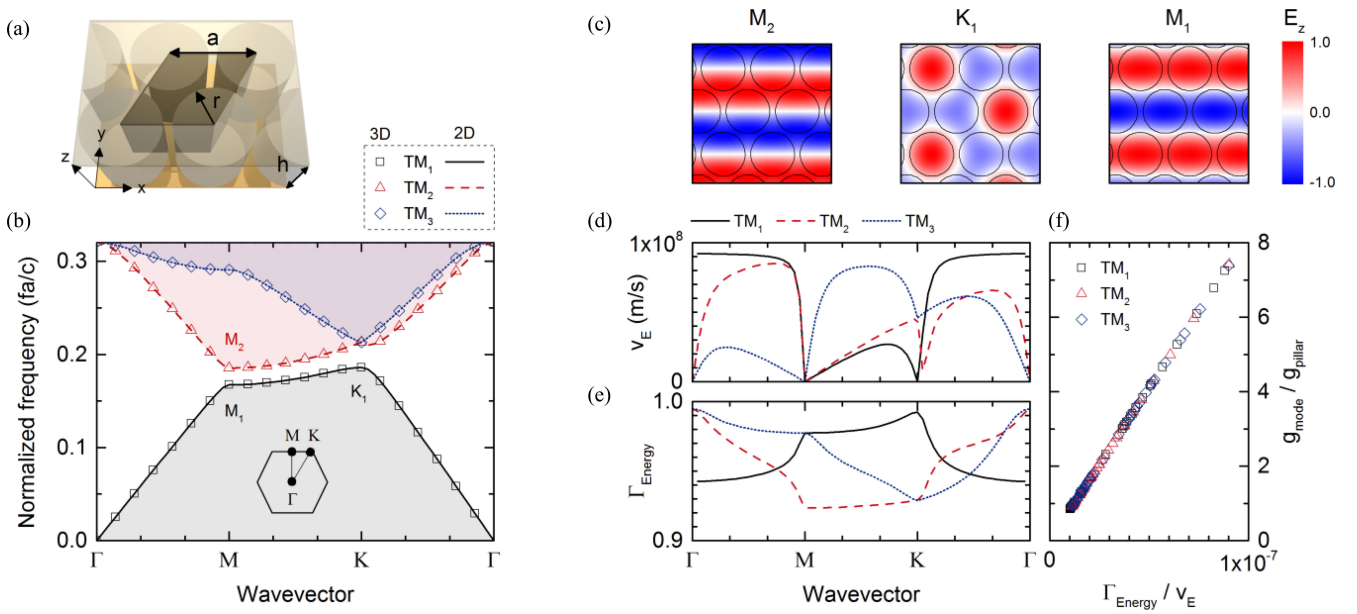

Fig. 2. Photonic band structure of active micropillar array terahertz lasers. (a) Unit cell of a hexagonal array of pillars embedded in a double-metal waveguide. (b) TM modes of GaAs pillars ($\varepsilon = 13.32$) in a BCB host material ($\varepsilon = 2.43$) with $r/a = 0.45$. Results are given for a 2-D calculation with infinitely long pillars, and a 3-D calculation with pillars embedded in a lossless double-metal waveguide with $r/h = 0.5$. (c) Normalized electric field distribution (E_z) in the *xy*-plane of TM modes at relevant high symmetry points. (d) Energy-transport velocity (v_E) of the calculated eigenmodes. (e) Electric field energy confinement (Γ_{Energy}) of each mode in the pillars. (f) Gain enhancement in the micropillar array characterized by the ratio between modal gain (g_{mode}) and material gain (g_{pillar}) in the active pillar material.

Fig. 2(d) and (e) present the calculated energy-transport velocity and the electric energy confinement of the modes, respectively. The electric field energy is strongly confined inside the pillars at the band edge (K_1) and saddle point (M_1) of the lowest band (TM_1), where the energy-transport velocity approaches zero. In active PhC structures the gain in the pillar medium can be significantly enhanced. As shown in Fig. 2(f), the gain enhancement, expressed by the ratio between the total modal gain (g_{mode}) and the local gain in the pillars (g_{pillar}), scales linearly with Γ_{Energy}/v_E [10].

As a result of the gain enhancement in the lossless PhC it is expected that lasing modes with a low group velocity and large mode confinement are selected. For micropillars embedded in a double metal waveguide, a low energy-transport velocity does not only enhance the interaction with the gain material but potentially also increases the losses in the metal layers. On the other hand, if during the device fabrication micropillar arrays are planarized with a lossy polymer for assembling the waveguide [27], a large mode confinement in the pillars also reduces the absorption losses in the planarization material.

B. Transparency Gain in Lossy PhCs

We have used the full 3-D finite-element model including material losses in the waveguide and planarization materials to calculate the minimum necessary intensity gain in the active pillar material in order to overcome existing losses. This transparency gain has been obtained for the three lowest TM bands of the periodic pillar array by minimizing the imaginary part of the respective complex eigenfrequencies. The materials have been modelled with a frequency dependent complex permittivity. For the calculations we have considered the materials we have used in our experiments. A Drude model with parameters fitted to experimental data has been used for modelling the frequency dependent complex permittivity of the gold waveguide layers [28]. The frequency dependent losses in the BCB host material are approximated using a linear model, which has been obtained from terahertz absorption measurements [26]. We have considered the same geometry as in the calculations of the lossless PhC. The ratio *r/a* has been kept constant at 0.45 and the waveguide (pillar) height has been set to 10 μm. The numerical results of the calculations are shown in Fig. 3. Eigenfrequencies and transparency gain values have been calculated for pillar diameters of 15.0 μm (see Fig. 3(a)), 12.5 μm (see Fig. 3(b)), and 10.0 μm (see Fig. 3(c)).

For the TM_1 band the transparency gain exhibits a pronounced local minimum at the K-point and a less pronounced minimum at the M-point independent of the pillar size. This is in agreement with the maxima of the gain enhancement in the lossless structure. For smaller wavevectors (approaching the Γ-Point), which correspond to lower frequencies, the metal as well as the polymer losses decrease, and as a result also the required gain in the pillar decreases. In general, the scaling of the micropillar array towards smaller dimensions shifts the eigenfrequencies to higher values. As a result the losses in the metal and the polymer are increased, which shifts the transparency gain curves to higher values.

Due to the high filling factor of the pillar array no pronounced photonic band gap is formed between the first and second TM band. Instead, only local gaps appear in the photonic band

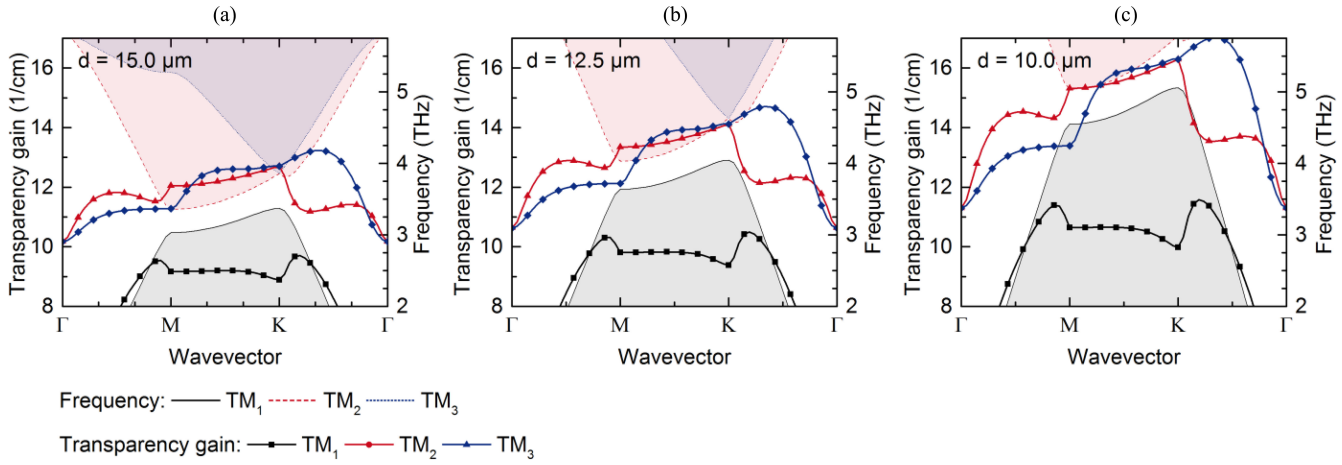

Fig. 3. Calculated transparency gain for active micropillar arrays in a polymer host material (BCB) embedded in a lossy double-metal waveguide (Au). The height of the waveguides has been 10 μm, and the r/a ratio has been kept constant at a value of 0.45. The eigenfrequencies of the TM_1, TM_2, and TM_3 bands, and the corresponding transparency gain values are plotted as a function of the wavevector (magnitude and direction) for pillar diameters of (a) 15.0 μm, (b) 12.5 μm, and (c)10.0 μm.

structure. In fact, the lowest eigenfrequency of the TM_2 band (M-Point) is very close to the highest eigenfrequency of the TM_1 band (K-Point). Depending on the pillar size this band edge is at 3.4, 4, or 5 THz. By comparing the values of the threshold gain at these two points it is however clear that the TM_1 mode requires significantly less gain.

In comparison to the gain enhancement in the lossless structure, the calculated transparency gain values illustrate the importance of frequency dependent losses for the operation of micropillar array terahertz lasers. The selection of lasing modes depends on the gain spectrum of the active medium and the threshold gain, which also takes mirror losses into account. In contrast to the photonic band structure, the gain spectrum of the pillar material is not influenced by the scaling of the pillar size. For pillar sizes where the band edge of the TM_1 band is sufficiently close to the gain maximum, micropillar array lasers will operate at the K-Point. By decreasing the pillar sizes, at some point a transition from lasing at the K-Point to lasing at the M-Point can be expected. For subwavelength micropillar arrays no pronounced minima in the transparency gain have been found. Therefore, lasing modes close to the gain maximum will dominate the emission spectrum.

III. Optical Feedback in Micropillar Arrays

In order to study the optical feedback mechanisms in micropillar array terahertz lasers, we have calculated the eigenmodes of finite, periodic pillar arrays with boundaries similar to a standard laser ridge. PhCs with a sufficient number of periods in both directions can be well approximated using periodic boundary conditions. In the case of PhCs with a small number of periods finite-size effects [29] have to be considered.

The micropillars are scaled in size, while the ratio of pillar radius to lattice spacing (*r/a*) is kept constant. The eigenmodes are again calculated using a finite element model for an array of GaAs pillars ($\varepsilon_{\mathrm{pillar}} = 13.32$ [25]) in a dielectric host of BCB ($\varepsilon_{\mathrm{host}} = 2.43$ [26]). In order to limit the computational complexity, the calculation is performed for a 2-D geometry, so the pillars are assumed to be infinitely long out-of-plane. This is a reasonable approximation for micropillar arrays embedded in double-metal waveguides in the case of a strong subwavelength confinement with electric field components almost independent of the z-direction.

For illustrating the transition from PhC modes to Fabry–Pérot (FP) modes we have extracted various eigenmodes at practically equal frequencies for different pillar diameters. In Fig. 4. the eigenmodes at a frequency of 4.0 THz are plotted for 500 μm $\times$ 150 μm large hexagonal arrays of micropillars with diameters of 12.7, 12.5, 11.4 μm, and 5 μm, and *r/a* ratio of 0.45. Due to finite-size effects various types of eigenmodes occur in these structures. For the analysis we have selected the closest eigenmodes to 4.0 THz.

With a pillar size of 12.7 μm an absolute frequency of 4.0 THz corresponds to a normalized frequency (*fa/c*) of 0.186, which is close to the band edge at the M-point of the second TM mode of the infinite array. In fact, the eigenmode at 4.0 THz of the finite pillar array shown in Fig. 4(a) agrees very well with the M-mode of the second TM band of the infinite array. Similarly, pillar sizes of 12.5 μm correspond to a normalized frequency of 0.183, which closely matches the K-point of the lowest TM band. For a diameter of 11.4 μm a frequency of 4 THz corresponds to $fa/c = 0.167$ which is close to the M-point of the first TM band. Consequently, the 4 THz eigenmode of the 12.5 μm diameter array shown in Fig. 4(b) resembles the K-mode of the infinite array, whereas the 4 THz eigenmode of the 11.4 μm array, shown in Fig. 4(c), is very similar to the mode at the M-point of the first TM band. These modes can therefore be considered to be mainly determined by the geometry of the PhC and can be approximated by the eigenmodes of the infinite pillar array.

On the contrary, for pillar diameters of 5 μm and the same relative lattice spacing, pillar dimensions are considerably smaller than the wavelength corresponding to 4 THz. The subwavelength pillar array therefore forms an effective medium for terahertz frequencies. The eigenmodes are given by the FP type resonator formed by the reflection at the boundaries due to the

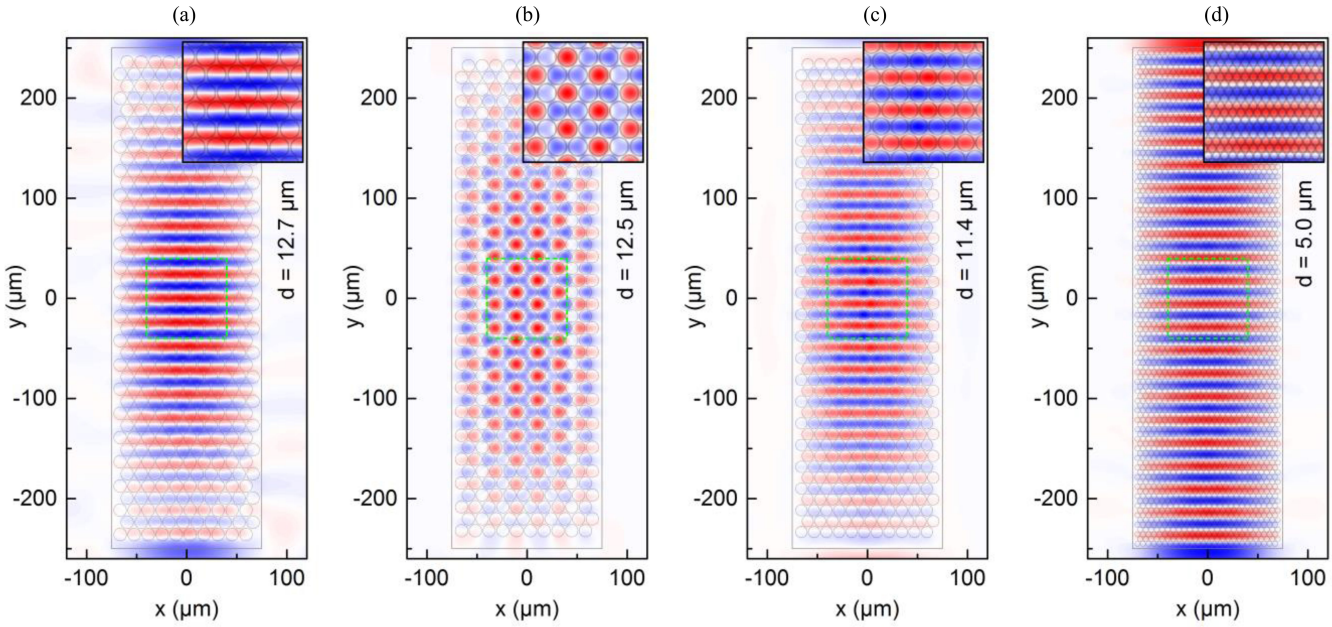

Fig. 4. Eigenmodes at 4.0 THz for finite-size 2-D micropillar arrays with dimensions of $500\,\mu\mathrm{m} \times 150\,\mu\mathrm{m}$. The GaAs pillars ($\varepsilon = 13.32$) are arranged on a hexagonal lattice ($r/a = 0.45$) and surrounded by a BCB host medium ($\varepsilon = 2.43$). Pillar diameters of (a) 12.7 μm, (b) 12.5 μm, (c) 11.4 μm, and (d) 5.0 μm are considered.

refractive index discontinuity. An eigenmode of the cavity close to 4.0 THz is shown in Fig. 4(d).

Depending on the pillar size relative to the eigenfrequency the respective modes are either mainly defined by the unit cell of the PhC or the boundary of the pillar array. For pillar sizes on the order of the wavelength, the diameter and spacing of the pillars defines the modes of the pillar array. If the pillar size is decreased to diameters far enough below the wavelength, a transition from these PhC modes to FP modes defined by the ridge geometry of the pillar array occurs.

IV. Experimental Results

We have fabricated a series of micropillar array devices with constant filling factor and varying pillar sizes similar to the structures theoretically analyzed in the previous sections. The emission spectra of these devices can be used to identify the transition from PhC modes to the effective medium regime. Varying the pillar spacing in the effective medium regime further allows determining the minimum necessary filling factors to achieve stimulated emission. This lower limit depends on the gain in the active region as well as the amount of waveguide losses present in the devices. It is not only relevant for the degree of freedom with respect to changing the refractive index of the effective gain medium, but also especially important for the successful realization of nanowire-based terahertz lasers.

A. Quantum Cascade Gain Medium

A terahertz quantum cascade structure with a three-well resonant phonon design has been used for the active pillar medium. The layer sequence of the active region is **4.5**/8.5/**2.8**/8.5/**4.5**/<u>16.4</u> nm, with $Al_{0.15}Ga_{0.85}As$ barriers indicated in bold and GaAs wells. This structure is a symmetric modification of a previously studied THz QCL design [30] with adapted extraction and injection barriers. The underlined 16.4 nm well has been doped with Si for a sheet doping density of $3.3 \times 10^{10}\,\mathrm{cm}^{-2}$. Previous investigations have shown a significant dependence of the device performance on the position of the doping [31]. The doping has therefore been shifted from the center of the 16.4 nm well in order to compensate the dopant migration during growth. The layer sequence, which is repeated 222 times yielding a total thickness of approximately 10 μm, has been grown using molecular beam epitaxy (MBE).

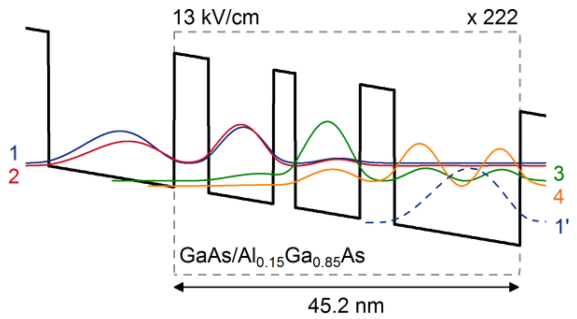

Fig. 5. Band structure of the active region at the design field of 13 kV/cm.

The bandstructure of the active region design is sketched in Fig. 5 for an applied electric field of 13.0 kV/cm (alignment field). Electrons are resonantly injected into the upper laser level (1→2) and resonantly extracted from the lower laser level (3→4). Longitudinal-optical phonon scattering of electrons into the next cascade efficiently depopulates the lower laser level (4→1′).

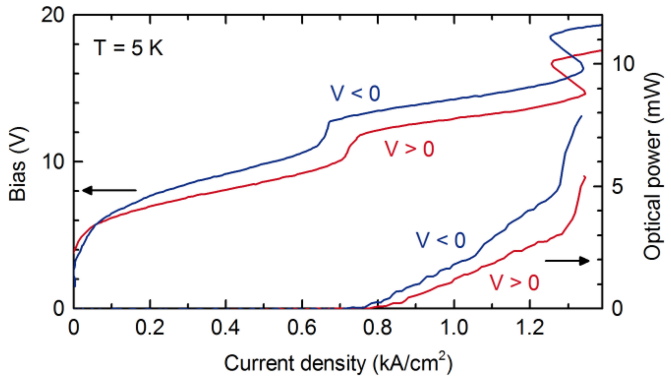

Fig. 6. LIV characteristics of a typical bulk laser ridge with a size of 1000 μm $\times$ 50 μm, which has been measured in pulsed mode at a heat sink temperature of 5 K.

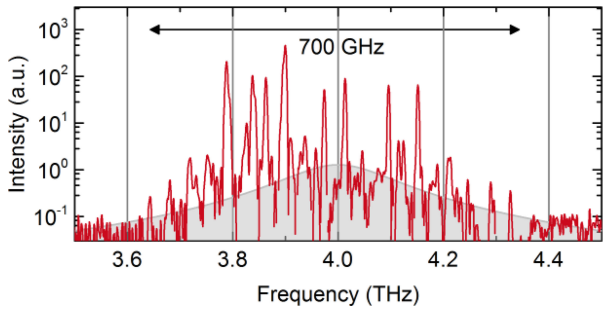

Fig. 7. Emission spectrum of a bulk laser ridge at the operating point of maximum output power. The output intensity is plotted on a logarithmic scale. The lasing modes approximately span from 3.65 to 4.35 THz covering a bandwidth of about 700 GHz. The grey curve in the background indicates a Lorentzian gain spectrum centered at 4.0 THz.

B. Reference Bulk Terahertz Lasers

In order to characterize the gain medium, we have fabricated regular bulk ridge laser devices with a double-metal waveguide. Due to the electrically symmetric design of the active region the devices can be operated either with a positive or negative bias. The performance in terms of threshold current density, maximum operating temperature, and optical output power differs for the two operating directions. The light–current–voltage (LIV) characteristics of a typical bulk device are given in Fig. 6 for both operating directions measured at a heat sink temperature of 5 K. The device has been operated in pulsed mode with a pulse length of 200 ns and a repetition frequency of 200 kHz. The measured threshold current density is approximately 0.8 kA/cm^2 for both operating directions. The peak output power varies between 8 mW for negative and 5 mW for positive bias. This difference in output power is the result of a higher optical gain for the negative bias direction. Although it is difficult to determine the exact value of optical gain in the active region, such a symmetric active region can be used for realizing pillar-based terahertz lasers, where the device behavior for the two operating directions with different optical gain can be directly compared.

In the studied micropillar array lasers the selection of lasing modes is determined by the optical gain spectrum of the active pillar medium. Fig. 7 shows the measured emission spectrum of a typical bulk device. The spectra were recorded at a heat sink temperature of 5 K and using a Fourier transform infrared spectrometer. The optical gain is centered approximately at 4 THz and spans over a bandwidth of roughly 700 GHz.

C. Micropillar Array Fabrication

Micropillar arrays with different pillar diameters and filling factors have been fabricated. The fabrication steps have been similar to standard terahertz PhC processing [27], which has also been previously used for the realization of subwavelength micropillar array lasers [15]. The MBE-grown active region as well as an additional GaAs substrate have been covered with Ti/Au metal layers and wafer bonded on top of each other. The substrate of the active region has then been removed using mechanical polishing and chemical wet etching. Micropillar arrays have been defined using electron beam lithography in order to achieve very high filling factors. A Ti/Au metal etch mask has been deposited using a lift-off technique. The active region has then been etched with a reactive ion etching machine using a highly anisotropic process [15]. The space in between the pillars has been filled up with BCB. Finally the top waveguide metal layers (Ti/Au) have been deposited and structured. The wafer pieces with the devices have been indium soldered to a copper holder and mounted in a cryostat.

D. Scaling of Micropillar Array Terahertz Lasers

Micropillar array terahertz lasers with pillar diameters ranging from 13.5 μm to 5.0 μm have been characterized. The micropillars have been arranged in a hexagonal array, with the ratio between pillar radius and lattice period (r/a) kept at a constant value of 0.45 for all devices. The relatively close spacing of the pillars yields a filling factor (η) of 0.75. The finite arrays of pillars form laser ridges with a typical size of 1000 μm $\times$ 200 μm. The devices were operated at a heat sink temperature of 5 K in pulsed mode with a typical repetition frequency of 20 kHz and pulse length of 500 ns.

The normalized emission spectra recorded at the operating point of maximum output power of selected micropillar array lasers are plotted in Fig. 8(a) on a normalized frequency scale (fa/c). The gain bandwidth of the active region (see Fig. 7) is depicted by the gray curve in the background of the emission spectra. As a reference, the corresponding photonic bands (TM modes) of the periodic structure are shown in Fig. 8(b). By decreasing the size (and period) of the pillars, the gain spectrum, which is centered at an absolute frequency of 4.0 THz, is shifted downwards on the normalized frequency scale. The normalized emission frequencies of devices with pillar diameters between 13.5 μm and 10.5 μm correspond to eigenmodes at high symmetry points of the photonic band diagram (M_1, K_1). On the contrary, micropillar array lasers with pillar diameters of 5 μm and 7 μm operate in the effective medium regime of the photonic band structure.

For pillar sizes that are large enough with respect to the emission wavelength of the active pillar material, the array forms a PhC laser. Lasing in these devices is not particularly preferred at the gain maximum of the active material, but the threshold gain

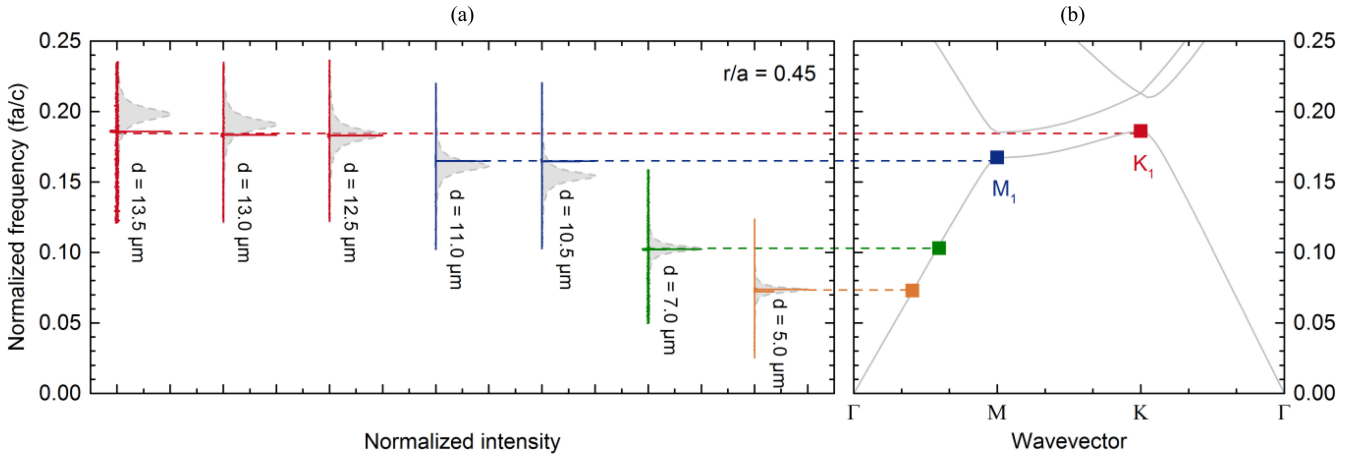

Fig. 8. Scaling of micropillar array terahertz lasers. (a) Measured emission spectra of micropillar array terahertz lasers with various pillar diameters on a normalized frequency scale. The ratio between pillar radius (diameter) and lattice spacing is kept constant at $r/a = 0.45$. The spectral range of the material gain is depicted by a Lorentzian function plotted in the background of the measurement data. (b) Calculated TM photonic band structure for a pillar array similar to the measured devices. Lasing emission for the larger pillar diameters (13.5 μm–10.5 μm) can be assigned to the high symmetry points of the TM_1 band (K_1, M_1), while devices with smaller pillar diameters (7 μm, 5 μm) operate in the effective medium regime of the photonic band structure.

for the different eigenfrequencies of the resonator is strongly influenced by the geometry of the PhC structure.

The highest gain enhancement and a minimum in the transparency gain has been calculated for the K-point at the band edge of the lowest TM band. In fact, with pillar diameters of 13.5, 13.0, and 12.5 μm, where the gain spectrum has some overlap with this band edge, lasing emission right at the K-point has been observed (left three spectra in Fig. 8(a)). All three micropillar array lasers have shown single mode emission at a normalized frequency (*fa/c*) of about 0.183. The electric field is strongly confined inside the pillars for this mode, with a field distribution corresponding to Fig. 4(b). The strong energy confinement in the active medium and the low energy-transport velocity results in the selection of this mode.

Scaling the pillar sizes to smaller diameters shifts the gain maximum away from the band edge towards the effective medium regime at the bottom end of the photonic band diagram. For diameters of 11.0 μm and 10.5 μm the normalized gain spectra are no longer overlapping with the band edge of the first TM band. However, a significant gain enhancement has been also calculated at the saddle point (M_1) of the first TM band. Similar to the band edge, the electric field energy is significantly confined inside the pillars and the energy-transport velocity goes to zero. As a result, single-mode lasing emission at the M-point has been observed for 11.0 μm and 10.5 μm micropillar sizes (see Fig. 8(a)). The corresponding optical mode of the micropillar array resonator is depicted in Fig. 4(c).

Further decreasing the pillar diameter shifts the gain spectrum into the effective medium regime of the band structure. In this case, the size of the pillars becomes considerably smaller than the optical wavelength and effectively a photonic metamaterial is formed. The electric field in this regime would be almost homogeneously distributed in an infinite array of micropillars. In the situation of a finite array in form of a laser ridge, the eigenmodes are similar to those of a bulk ridge laser, and therefore defined by the refractive index contrast at the boundary of the array as shown in Fig. 4(d). The emission of micropillar arrays lasers in the effective medium regime with pillar diameters of 7.0 and 5.0 μm is centered at the gain maximum of the active region and usually no longer single mode (two rightmost spectra in Fig. 8(a)).

The corresponding emission spectra with absolute frequency values and a logarithmic intensity scale of the different micropillar array lasers are shown in Fig. 9. In the case of PhC lasers (see Fig. 9(a)–(e)), scaling the pillar sizes to smaller dimensions has shifted the absolute emission frequency to higher values. Depending on the pillar diameter single mode emission frequencies have been varied over a range of more than 500 GHz between 3.75 THz for a diameter of 13.5 μm and 4.28 THz for 10.5 μm large pillars. Subwavelength micropillar array devices with pillar diameters of 7.0 μm and 5.0 μm (see Fig. 9(f) and (g)) operated preferentially close to the gain maximum. Depending on the device, one or more optical modes have been observed in the emission spectrum.

Although the PhC laser devices only operated at two different points (M, K) of the photonic bands on the normalized frequency scale, the absolute lasing frequency can be shifted almost over the whole spectral gain bandwidth. The single mode emission lasing frequency is defined by the geometry of the PhC, and therefore makes such structures very useful for frequency tuning. Dedicated broadband active region designs would allow frequency tuning over an even further range. The best performance, however, can be achieved for devices with an emission frequency close to the gain maximum. For small pillar diameters the gain spectrum no longer overlaps with the band edge (K_1) or saddle point (M_1) of the first photonic band, and lasing emission is no longer favored at a certain normalized frequency.

In addition to the coarse tuning by the pillar array geometry, a fine tuning of the lasing frequency can be achieved by changing the applied bias [3]. Fig. 10 shows the normalized emission

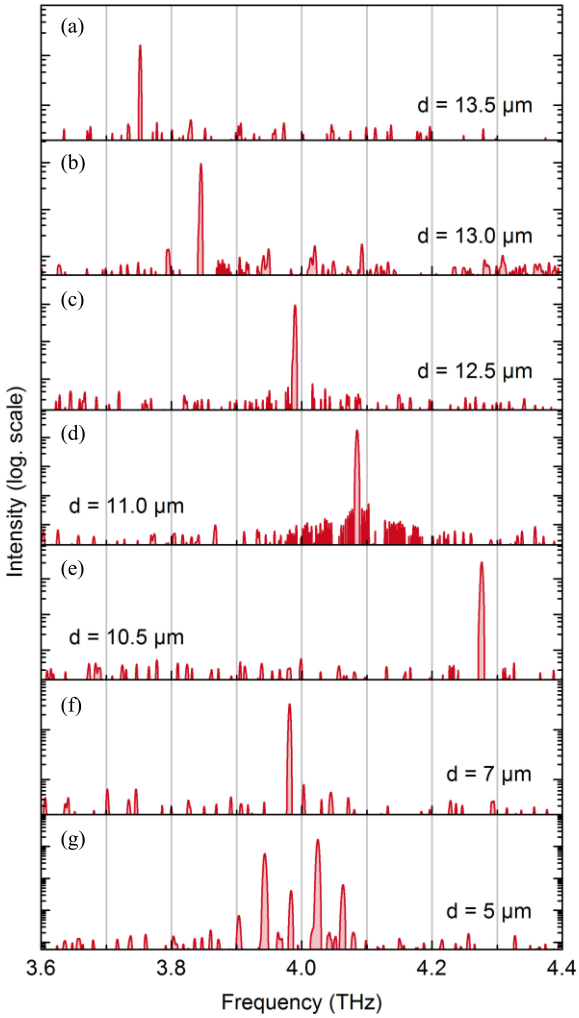

Fig. 9. Tuning the lasing frequency by scaling the pillar diameter. While single mode emission at high symmetry points is favored in PhC devices (a)–(e), subwavelength micropillar array lasers (f), (g) emit close to the gain maximum of the active region.

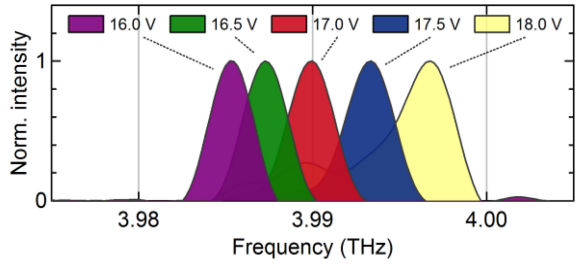

Fig. 10. Normalized emission spectra of the 12.5 μm device for different applied biases (negative polarity). The lasing frequency is shifted by approximately 10 GHz.

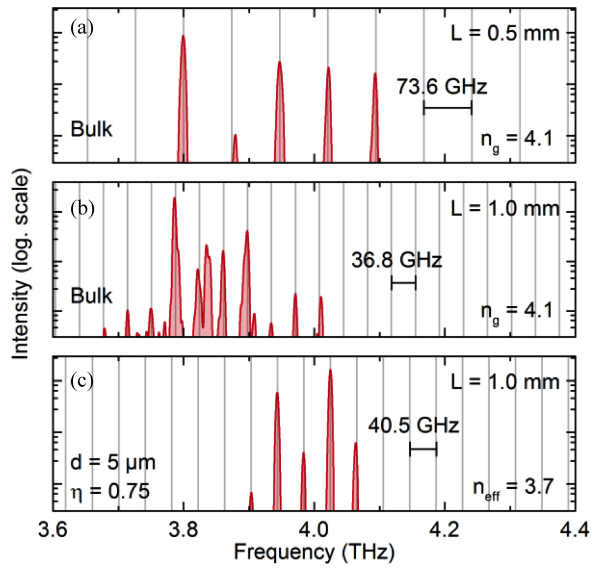

Fig. 11. Comparison between emission spectra of (a), (b) bulk laser ridges with different cavity lengths (0.5 mm, 1 mm) and (c) a subwavelength micropillar array laser with 5 μm pillars and a filling factor of 0.75. The group index (n_g) of the bulk gain medium and the effective group index (n_{eff}) of the micropillar array medium is extracted from the measured longitudinal mode spacing.

spectra of a PhC laser with 12.5 μm large pillars as a function of the applied bias. The emission frequency is tuned over a range of approximately 10 GHz.

The longitudinal mode spacing in the effective medium regime is given by the group index of the effective medium. In Fig. 11 the emission spectra of two bulk devices with cavity lengths of 0.5 mm (seeFig. 11(a)) and 1.0 mm (see Fig. 11(b)), and a subwavelength micropillar array laser with pillar diameters of 5 μm, filling factor of 0.75, and a length of 1 mm (see Fig. 11(c)) are shown. The mode spacing between adjacent longitudinal modes is indicated in the figure. The longitudinal mode spacing of the bulk devices yields a group index of $n_g = 4.1$. Compared to the 0.5 mm long laser cavity, the 1.0 mm long bulk device has precisely half the longitudinal mode spacing. This results from the difference in the optical path lengths of the two bulk laser cavities. The longitudinal mode spacing of 40.5 GHz for the 1.0 mm long subwavelength micropillar device yields a reduced effective group index of the micropillar array of $n_{\text{eff}} = 3.7$. This agrees well with the lower refractive index in the host material and the filling factor of the array.

E. Terahertz Emission at Varying Filling Factors

Limitations of subwavelength micropillar array lasers have been studied by varying the filling factor of the pillar array. Devices with 5 μm pillar diameters, total array sizes between 1000 μm $\times$ 120 μm and 1000 μm $\times$ 200 μm, and filling factors between 0.75 and 0.65 have been fabricated and characterized. For the sensitive measurement of the spontaneous terahertz emission of non-lasing micropillar arrays we have used a liquid helium cooled p-doped germanium detector. The emitted terahertz radiation has been collected by a hollow copper tube and guided to the detector [32]. The devices have been operated in pulsed mode with 500 ns long pulses and a repetition frequency of 100 kHz. This pulse train has been modulated with a frequency of 10 Hz, and the optical emission has been measured by sensing the change in resistance of the p-Ge detector with a lock-in amplifier locked to the modulation frequency.

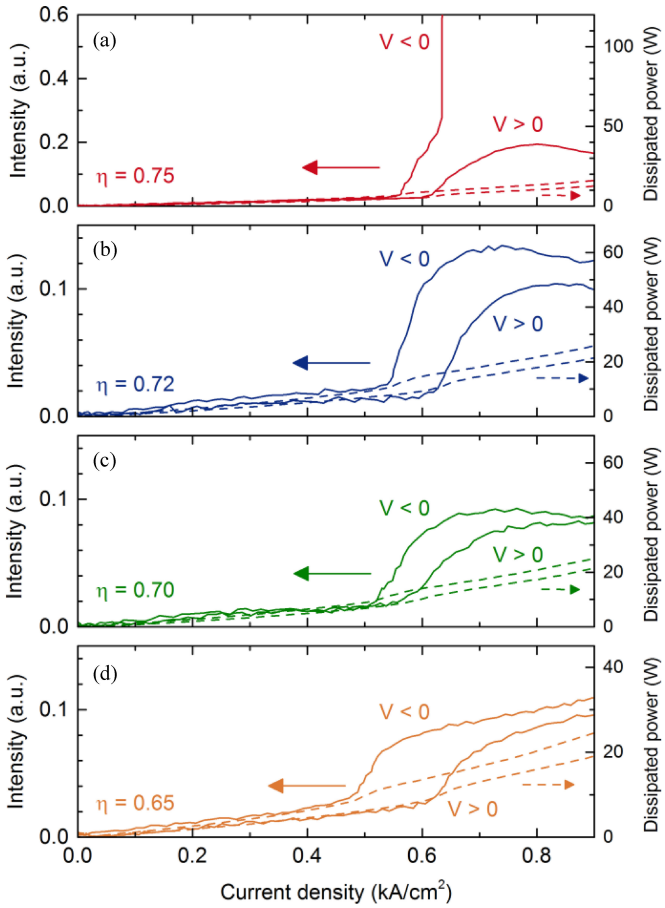

Fig. 12. Emission measurements for micropillar arrays with diameters of 5 μm and filling factors of (a) 0.75, (b) 0.72, (c) 0.70, and (d) 0.65. At low current densities (<0.5 kA/cm^2) the measured emission scales with the peak dissipated electrical power (indicated by dashed lines). With the onset of injection of electrons into the upper laser level a steep increase in the emission is observed for all devices. Lasing, however, is only observed for a filling factor of 0.75 and a negative applied bias.

Emission measurements for micropillar arrays with different filling factors are presented in Fig. 12. The given values of the current density correspond to the average current density in the pillars, neglecting any effects of surface depletion [15]. At low current densities, which correspond to a low applied bias, electrons are injected into the lower laser level and practically no terahertz radiation is emitted. The measured emission for current densities below 0.5 kA/cm^2 scales with the dissipated power in the devices, and therefore stems from the current induced heating of the micropillars. The peak dissipated power is indicated by dashed lines in the figure. The thermal emission, which scales with the duty cycle of the pulsed operation, represents a background to the emitted terahertz radiation. With the start of injection into the upper laser level at current densities above 0.5 kA/cm^2, corresponding to an increase in the applied bias, a steep increase in the emission has been measured. This increase no longer scales with the dissipated power in the device and is attributed to the emission of terahertz radiation. The gain of the active pillar medium is however not yet sufficient to achieve stimulated emission at this point. The onset of the spontaneous emission occurs between 0.5 and 0.6 kA/cm^2 and depends on the operating direction of the device. Similar to the bulk devices, in positive operating direction a higher current density is required to reach alignment with the upper laser level.

Stimulated emission has been observed only for the maximum filling factor of 0.75 and a negative applied bias as shown in Fig. 12(a). This micropillar array device had a total size of $1000\,\mu\mathrm{m} \times 120\,\mu\mathrm{m}$ and a lattice spacing of 5.5 μm. A strong increase in the output power has been measured with the onset of lasing at 0.64 kA/cm^2. In positive operating direction the optical gain of the pillar array is not sufficient to overcome waveguide and mirror losses. The roll-over point of maximum emission is at 0.8 kA/cm^2. In case of lower filling factors (Fig. 12(b)–(d)), spontaneous terahertz emission has been measured but no onset of lasing is observed. The sizes of the pillar arrays are $1000\,\mu\mathrm{m} \times 200\,\mu\mathrm{m}$ and lattice spacings are 5.6, 5.7 and 5.9 μm. The lower the filling factor, the lower the gain in the effective pillar medium and therefore stimulated emission is more difficult to achieve. In addition, the measured emission intensity decreased with a reduction in the pillar density.

If the pillars are scaled to nanowire dimensions with a lateral electron confinement, the nanowire array effectively forms a quantum dot ensemble [20]. In principle, it is expected that for such a dense array of emitters with a spacing much smaller than the emission wavelength, the emitters become coherently coupled with the result of a significantly enhanced spontaneous emission rate [33], [34].

Terahertz PhC lasers have been previously realized for filling factors as low as 0.33 with empty space between the pillars [4] and 0.4 using a lossy BCB host material [3]. In the PhC regime the observed lasing modes are strongly confined in lateral direction inside the active pillar medium, which significantly increases the effective filling factor [15]. In the effective medium regime, in contrast, the electric field is uniformly distributed between pillar and host medium. As a result, significantly higher filling factors are required for a lasing operation in the effective medium regime. The fabricated subwavelength array micropillar lasers have been limited by waveguide losses to a minimum required filling factor of 0.75. First, a larger amount of planarization material increases the absorption losses, and second a smaller amount of active material reduces the total optical gain. In addition, waveguide losses can also increase due to rough waveguide layers resulting from the pillar array planarization. A scaling of pillar arrays towards nanowire dimensions critically depends on the ability to reduce these losses.

V. Waveguide Losses in Subwavelength Micropillar Array Terahertz Lasers

We have analyzed the relationship between waveguide losses in subwavelength micropillar array devices and the amount of optical gain in the active pillar material, which is necessary to overcome these losses. The eigenmodes of the waveguide have been calculated using a 3-D finite element model with Bloch periodic boundary conditions. We have restricted the analysis to eigenmodes with a propagation in y-direction (corresponds to the Γ-M direction in the photonic band diagram) in

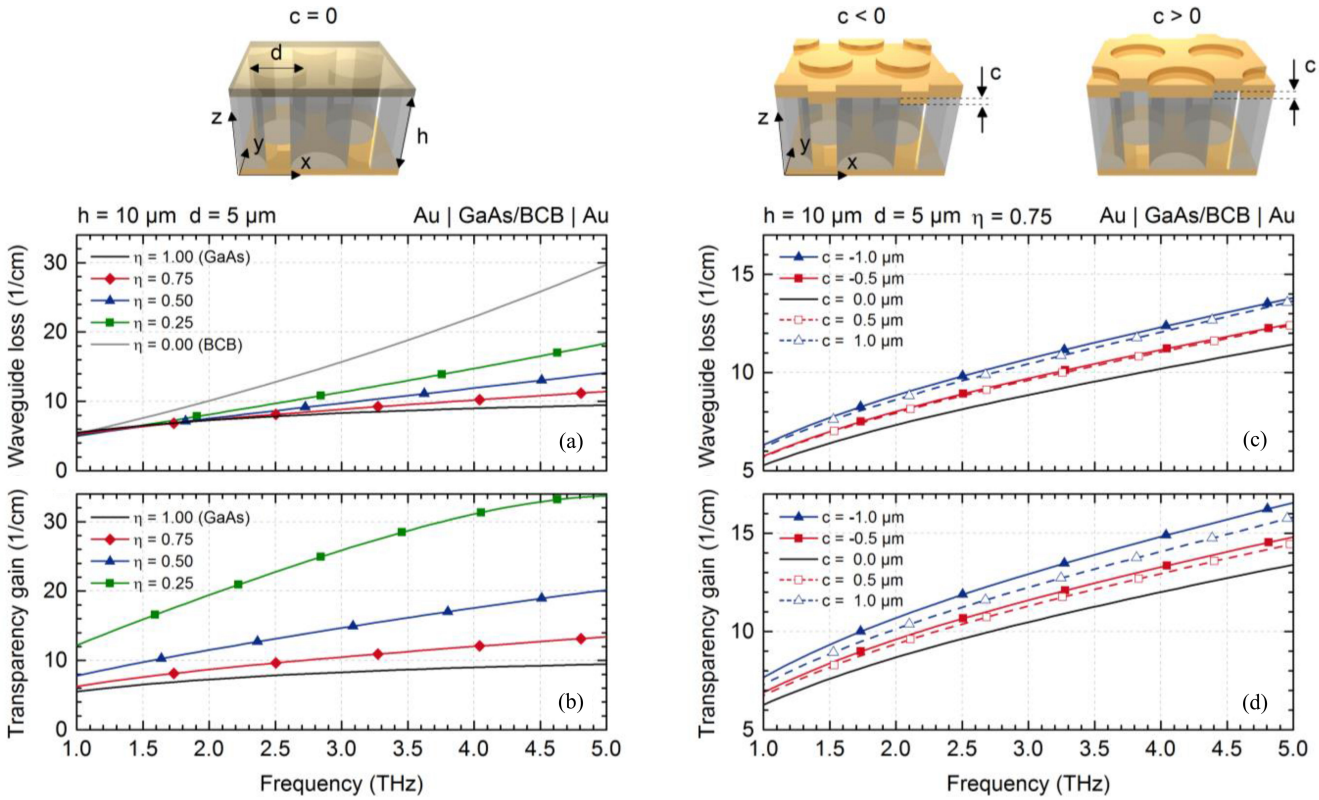

Fig. 13. Influence of filling factor and waveguide roughness on waveguide losses and transparency gain of subwavelength micropillar array terahertz lasers. The calculations have been performed for a hexagonal array of GaAs pillars with 5 μm diameter in a BCB host medium and embedded in a 10 μm high gold-gold waveguide. (a) Waveguide loss and (b) transparency gain for different pillar array filling factors in case of a perfectly flat double-metal waveguide. As a reference, data for waveguides filled with bulk GaAs and BCB is given. (c) Waveguide loss and (d) transparency gain of micropillar arrays in a double-metal waveguide with a two-dimensional corrugation height (c) of the top waveguide layer. The filling factor of the micropillar arrays has been 0.75.

accordance with the geometry of the experimentally realized devices. The frequency dependent losses have been taken into account by the complex permittivity of BCB, which has been approximated using a linear fit to experimentally determined values in the terahertz range [26], and a Drude model for the gold waveguide layers [28]. In a terahertz QCL active region the free carrier absorption can be considered to be very small [35]. Consequently, the pillar medium has been assumed to be free of absorption losses in the calculation of the waveguide losses. The transparency condition for each propagating mode has been found by adjusting the complex anisotropic permittivity tensor that determines the optical gain in the pillar medium.

A. *Influence of Filling Factor*

The filling factor determines not only the amount of active material in the device but also the waveguide loss. The influence of the filling factor on the waveguide loss and the transparency gain has been studied for GaAs micropillar arrays in a BCB host material and a gold-gold waveguide. The calculations have been performed for a pillar diameter of 5 μm and a pillar height of 10 μm. The results of these calculations are shown in Fig. 13(a) and (b).

In general, waveguide losses (see Fig. 13(a)) increase with frequency as a result of the increased losses in the metal waveguide layers and the polymer host material. The waveguide loss also significantly increases for small filling factors. Even though BCB has relatively low losses in the terahertz range, a large amount of BCB in the waveguide considerably increases the losses. This can be clearly seen by comparing double-metal waveguides filled with GaAs to waveguides completely filled with BCB. For frequencies above 4 THz the waveguide loss increases by more than a factor of two.

The necessary optical gain in the pillar medium in order to overcome the waveguide losses is shown in Fig. 13(b). In a standard bulk double-metal waveguide the amount of gain in the active region necessary to overcome the waveguide loss approximately equals the waveguide loss. This is due to the fact that the mode confinement factor is approximately one in this case. However, in the micropillar array medium the gain is not homogeneously distributed but localized in the pillars. Especially for low filling factors this transparency gain significantly exceeds the value of the waveguide loss. However, it does not increase by a factor of four in the case of a filling factor of 0.25 as one might naively expect. It is the concentration of the electric field energy in the pillar medium that enhances the optical gain of the micropillar even in the effective medium regime.

B. *Influence of Top Waveguide Layer Roughness*

Another relevant aspect of the waveguide design that needs to be considered is the influence of the roughness of the

waveguide layers. In the fabrication of the micropillar array lasers, the bottom waveguide layer is formed by wafer-bonding which results in an almost perfectly flat layer. However, the top waveguide layer is formed after planarization of the pillar array. If the planarization material does not completely fill up the space between the pillars, or if a metal etch mask layer remains on top of the pillars, a top waveguide layer with a 2-D corrugation is the result. It has been previously shown that a deep subwavelength 1-D corrugation of the metal layers can strongly alter the dispersion [36]. We have studied the influence of rather shallow corrugations on the waveguide losses.

Fig. 13(c) and (d) shows the increase in waveguide losses and transparency gain with an increase in surface roughness (c) for a micropillar array with 5 μm large pillars and a filling factor of 0.75. The height of the pillars has been fixed to 10 μm. Waveguide losses (see Fig. 13(c)) significantly increase for a step size of 1 μm, and are also relevant for smaller corrugations. The change in waveguide losses is relatively similar for positive and negative corrugations. However, the transparency gain (see Fig. 13(d)) is higher for negative corrugations ($c < 0$) compared to positive ones ($c > 0$). In the case of a negative corrugation the mode is pushed into a smaller volume reducing its overlap with the pillars.

The corrugation heights assumed in the calculations are rather high. Typical values for fabricated micropillar array lasers have been below 200 nm. It can therefore be assumed that the increase of waveguide losses due to the surface roughness of the top waveguide layer has a rather minor influence on the device performance.

VI. Conclusion

We have demonstrated the scaling of active pillar arrays with high packing densities for the realization of terahertz PhC lasers and subwavelength micropillar array lasers. Although no photonic band gap is formed, single mode emission across the spectral gain bandwidth has been achieved. In principle, PhC lasers can also be realized with lower filling factors, but effective medium devices are still limited to high filling factors. The operation of subwavelength pillar array devices with lower filling factors has been restricted by additional losses introduced by the planarization material and the roughness of the top waveguide layer. In order to overcome this limitation, the use of planarization materials with lower losses, or avoiding such materials at all will be beneficial. However, the mechanical stability of such free standing structures will have to be ensured. Especially for very small diameters in the nanowire range, high filling factors are increasingly difficult to realize, but necessary for the realization of nanowire-based terahertz lasers.

References

[1] J. B. Wright *et al.*, "Multi-colour nanowire photonic crystal laser pixels," *Sci. Rep.*, vol. 3, p. 2982, Oct. 2013.

[2] H. Matsubara *et al.*, "GaN photonic-crystal surface-emitting laser at blue-violet wavelengths," *Science*, vol. 319, no. 5862, pp. 445–447, Jan. 2008.

[3] H. Zhang, L. A. Dunbar, G. Scalari, R. Houdré, and J. Faist, "Terahertz photonic crystal quantum cascade lasers," *Opt. Exp.*, vol. 15, no. 25, pp. 16818–16827, Dec. 2007.

[4] A. Benz *et al.*, "Active photonic crystal terahertz laser," *Opt. Exp.*, vol. 17, no. 2, pp. 941–946, Jan. 2009.

[5] Y. Chassagneux *et al.*, "Electrically pumped photonic-crystal terahertz lasers controlled by boundary conditions," *Nature*, vol. 457, no. 7226, pp. 174–178, Jan. 2009.

[6] L. A. Dunbar *et al.*, "Design, fabrication and optical characterization of quantum cascade lasers at terahertz frequencies using photonic crystal reflectors," *Opt. Exp.*, vol. 13, no. 22, pp. 8960–8968, Oct. 2005.

[7] A. Benz *et al.*, "Terahertz photonic crystal resonators in double-metal waveguides," *Opt. Exp.*, vol. 15, no. 19, pp. 12418–12424, Sep. 2007.

[8] O. Painter *et al.*, "Two-dimensional photonic band-gap defect mode laser," *Science*, vol. 284, no. 5421, pp. 1819–1821, Jun. 1999.

[9] R. Colombelli *et al.*, "Quantum cascade surface-emitting photonic crystal laser," *Science*, vol. 302, no. 5649, pp. 1374–1377, Nov. 2003.

[10] S. Nojima, "Optical-gain enhancement in two-dimensional active photonic crystals," *J. Appl. Phys.*, vol. 90, no. 2, pp. 545–551, Jul. 2001.

[11] B. S. Williams, "Terahertz quantum-cascade lasers," *Nat. Photon.*, vol. 1, no. 9, pp. 517–525, Sep. 2007.

[12] M. Bahriz, V. Moreau, R. Colombelli, O. Crisafulli, and O. Painter, "Design of mid-IR and THz quantum cascade laser cavities with complete TM photonic bandgap," *Opt. Exp.*, vol. 15, no. 10, pp. 5948–5965, May 2007.

[13] H. Zhang, G. Scalari, M. Beck, J. Faist, and R. Houdré, "Complex-coupled photonic crystal THz lasers with independent loss and refractive index modulation," *Opt. Exp.*, vol. 19, no. 11, pp. 10707–10713, May 2011.

[14] A. Benz *et al.*, "Photonic bandstructure engineering of THz quantum-cascade lasers," *Appl. Phys. Lett.*, vol. 99, no. 20, p. 201103, Nov. 2011.

[15] M. Krall *et al.*, "Subwavelength micropillar array terahertz lasers," *Opt. Exp.*, vol. 22, no. 1, pp. 274–282, Jan. 2014.

[16] J. Faist *et al.*, "Quantum cascade laser," *Science*, vol. 264, no. 5158, pp. 553–556, Apr. 1994.

[17] R. Köhler *et al.*, "Terahertz semiconductor-heterostructure laser," *Nature*, vol. 417, no. 6885, pp. 156–159, May 2002.

[18] S. Kumar, C. W. I. Chan, Q. Hu, and J. L. Reno, "A 1.8-THz quantum cascade laser operating significantly above the temperature of $\hbar\omega/k_{\mathrm{B}}$," *Nat. Phys.*, vol. 7, no. 2, pp. 166–171, Feb. 2011.

[19] Y. Chassagneux *et al.*, "Limiting factors to the temperature performance of THz quantum cascade lasers based on the resonant-phonon depopulation scheme," *IEEE Trans. Terahertz Sci. Technol.*, vol. 2, no. 1, pp. 83–92, Jan. 2012.

[20] C.-F. Hsu, J.-S. O, P. Zory, and D. Botez, "Intersubband quantum-box semiconductor lasers," *IEEE J. Sel. Top. Quantum Electron.*, vol. 6, no. 3, pp. 491–503, Jun. 2000.

[21] D. Smirnov *et al.*, "Control of electron–optical-phonon scattering rates in quantum box cascade lasers," *Phys. Rev. B*, vol. 66, no. 12, p. 121305, Sep. 2002.

[22] T. Grange, "Nanowire terahertz quantum cascade lasers," *Appl. Phys. Lett.*, vol. 105, no. 14, p. 141105, Oct. 2014.

[23] M. I. Amanti *et al.*, "Electrically driven nanopillars for THz quantum cascade lasers," *Opt. Exp.*, vol. 21, no. 9, pp. 10917–10923, May 2013.

[24] T. Frost *et al.*, "Monolithic electrically injected nanowire array edge-emitting laser on (001) silicon," *Nano Lett.*, vol. 14, no. 8, pp. 4535–4541, Aug. 2014.

[25] H. Yasuda and I. Hosako, "Measurement of terahertz refractive index of metal with terahertz time-domain spectroscopy," *Jpn. J. Appl. Phys.*, vol. 47, no. 3, pp. 1632–1634, Mar. 2008.

[26] E. Perret, N. Zerounian, S. David, and F. Aniel, "Complex permittivity characterization of benzocyclobutene for terahertz applications," *Microelectron. Eng.*, vol. 85, no. 11, pp. 2276–2281, Nov. 2008.

[27] H. Zhang, G. Scalari, J. Faist, L. A. Dunbar, and R. Houdré, "Design and fabrication technology for high performance electrical pumped terahertz photonic crystal band edge lasers with complete photonic band gap," *J. Appl. Phys.*, vol. 108, no. 9, p. 093104, Nov. 2010.

[28] M. A. Ordal, R. J. Bell, R. W. Alexander, L. L. Long, and M. R. Querry, "Optical properties of fourteen metals in the infrared and far infrared: Al, Co, Cu, Au, Fe, Pb, Mo, Ni, Pd, Pt, Ag, Ti, V, and W," *Appl. Opt.*, vol. 24, no. 24, pp. 4493–4499, Dec. 1985.

[29] S. Nojima, "Theoretical analysis of feedback mechanisms of two-dimensional finite-sized photonic-crystal lasers," *J. Appl. Phys.*, vol. 98, no. 4, p. 043102, Aug. 2005.

[30] S. Kumar, Q. Hu, and J. L. Reno, "186 K operation of terahertz quantum-cascade lasers based on a diagonal design," *Appl. Phys. Lett.*, vol. 94, no. 13, p. 131105, Apr. 2009.

[31] C. Deutsch *et al.*, "Dopant migration effects in terahertz quantum cascade lasers," *Appl. Phys. Lett.*, vol. 102, no. 20, p. 201102, May 2013.
[32] M. Brandstetter *et al.*, "Reversing the pump dependence of a laser at an exceptional point," *Nat. Commun.*, vol. 5, p. 4034, Jun. 2014.
[33] R. H. Dicke, "Coherence in spontaneous radiation processes," *Phys. Rev.*, vol. 93, no. 1, pp. 99–110, Jan. 1954.
[34] M. Scheibner *et al.*, "Superradiance of quantum dots," *Nat. Phys.*, vol. 3, no. 2, pp. 106–110, Feb. 2007.
[35] F. Carosella *et al.*, "Free-carrier absorption in quantum cascade structures," *Phys. Rev. B*, vol. 85, no. 8, p. 085310, Feb. 2012.
[36] M. A. Kats, D. Woolf, R. Blanchard, N. Yu, and F. Capasso, "Spoof plasmon analogue of metal-insulator-metal waveguides," *Opt. Exp.*, vol. 19, no. 16, pp. 14860–14870, Aug. 2011.

Michael Krall studied electrical engineering at the Vienna University of Technology and the University of Illinois, Urbana-Champaign, and received the Diploma degree in microelectronics from the Vienna University of Technology, Vienna, Austria, in 2009.

From 2009 to 2010, he was a Fulbright Fellow with the Nanoelectronics Research Lab, University of California, Santa Barbara, CA, USA, where he investigated quantum transport phenomena in graphene-based nanoelectronic devices. He is currently a Research Assistant with the Photonics Institute, Vienna University of Technology, Vienna, Austria. His research interests include generation and detection of terahertz radiation with quantum-engineered semiconductor heterostructures.

Martin Brandstetter received the Dipl.-Ing. and Ph.D. degrees in 2010 and 2014, respectively, from the Photonics Institute, Vienna University of Technology, Vienna, Austria, for his work on novel cavity concepts for terahertz quantum cascade lasers.

His current research interests include the improvement of the performance of terahertz quantum cascade lasers and the investigation of photonic and plasmonic phenomena using these devices.

Christoph Deutsch received the Ph.D. degree for his work on quantum cascade lasers from the Vienna University of Technology, Vienna, Austria, in 2013.

During the Ph.D. studies, he joined the Walter–Schottky–Institute, TU München, and the Electrical Engineering Department, Princeton University as a visiting Researcher. He is currently a Postdoctoral Fellow at the Photonics Institute, Vienna University of Technology, and his current research interests include material aspects and high output powers in the field of terahertz quantum cascade lasers.

Hermann Detz received the Master's degree in electrical engineering from the Vienna University of Technology, Vienna, Austria, in 2007, investigating second-harmonic generation in quantum cascade lasers, and the Ph.D. degree for developing InGaAs/GaAsSb heterostructures for quantum cascade lasers in 2011.

He has stayed with the Vienna University of Technology as a Postdoctoral researcher. Since 2015, he has been an APART Fellow of the Austrian Academy of Sciences, Wien, Austria. His current research interests include the growth of optoelectronic intersubband devices, low-dimensional nanostructures, and novel materials by molecular beam epitaxy as well as atomistic modeling of semiconductor materials. He is author or coauthor of more than 50 peer-reviewed publications and of more than 200 conference contributions.

Aaron Maxwell Andrews received the B.S. degree in materials science and engineering from the University of California, Los Angeles, CA, USA, in 1997, and the Ph.D. degree in materials engineering from the University of California, Santa Barbara, CA, USA, in 2003.

Since 2004, he has been at the Vienna University of Technology, Vienna, Austria, working on the development of mid-infrared and terahertz quantum cascade lasers, intersubband detectors, quantum dots, polariton heterostructures, nanowires, strain compensation, and the growth of novel materials by molecular beam epitaxy. He is author or coauthor of more than 130 scientific publications and 400 conference contributions.

Werner Schrenk studied physics at the Vienna University of Technology (TU Vienna), Vienna, Austria, and received the Dipl.-Ing. degree in 1997, and the Ph.D. degree from the Solid State Electronics Institute, TU Vienna, in 2001.

Since 2001, he has been the Technical Director of the cleanroom of the Center for Micro- and Nanostructures, TU Vienna.

Gottfried Strasser received the Ph.D. degree in physics from the University of Innsbruck, Innsbruck, Austria, in 1991, and the State Doctorate degree from the Vienna University of Technology (TU Vienna), Vienna, Austria in 2001.

From 1988 to 1992, he was a Research Assistant at the Technical University Munich, Munich, Germany. In 1992, he became an Assistant Professor, and in 2001, an Associate Professor at the Vienna University of Technology, Vienna, Austria. In 2007, he became a full Professor at the State University of New York, Buffalo, NY, USA, where he was an Empire Innovation Professor with the Department of Electrical Engineering and the Department of Physics. Since March 2009, he has been a full Professor at the TU Vienna in Austria, where he started heading the Center for Micro- and Nanostructures in 2012. He has authored or coauthored 400 journal papers, 290 conference papers, and more than 1100 conference contributions in the related areas. His current research interests include growth and processing of III–V semiconductors for photonic and electronic applications.

Karl Unterrainer received the M.S. degree in physics and the Ph.D. degree for his work on stimulated far infrared emission from the University of Innsbruck, Innsbruck, Austria, in 1986 and 1989, respectively.

Subsequently, he worked as a Research Assistant at the Institute for Experimental Physics and developed a far infrared tunable cyclotron resonance laser. In 1992, he became an Assistant Professor at the Technical University Vienna, Vienna, Austria. In 1994 and 1995, he worked as a Visiting Researcher at the Quantum Institute, University of California, Santa Barbara, CA, USA. He used nonlinear terahertz spectroscopy to study intersubband relaxation rates and observed the inverse Bloch oscillator effect. From 1997 till 2003, he was an Associate Professor at the Technical University Vienna. Since 2004, he has been a full Professor at the Photonics Institute, Technical University Vienna. Since 2006, he is coordinating the FWF research cluster "Infrared Optical Nanostructures IR-ON." His main research interests include terahertz spectroscopy of semiconductor nanostructures and the development of nanophotonic devices. He is author or coauthor of more than 250 scientific articles.